

Do $z > 6$ quasars reside in protoclusters?

Fabio Fontanot^{1,2,*,}, Roberto Decarli³, Gabriella De Lucia^{1,2}, Olga Cucciati³, Lizhi Xie⁴, and Michaela Hirschmann^{5,1}

¹ INAF - Astronomical Observatory of Trieste, via G.B. Tiepolo 11, I-34143 Trieste, Italy

² IFPU - Institute for Fundamental Physics of the Universe, via Beirut 2, 34151, Trieste, Italy

³ INAF - Osservatorio di Astrofisica e Scienza dello Spazio di Bologna, Via Piero Gobetti 93/3, 40129 Bologna, Italy

⁴ Tianjin Astrophysics Center, Tianjin Normal University, Binshuixida 393, 300384, Tianjin, China

⁵ EPFL - Institute for Physics, Laboratory for Galaxy Evolution, Observatoire de Sauverny, Chemin Pegasi 51, 1290 Versoix, Switzerland

Received ???, 2024; accepted ???, 2024

ABSTRACT

We discuss the properties of a sample of $z > 6$ bright (bolometric luminosity $L_{\text{bolo}} > 10^{46.25}$ erg/s) Quasars drawn from a realization of the Galaxy Evolution and Assembly (GAEA) model coupled with the Planck Millennium Simulation. We focus on the properties and environment of host galaxies, and their evolution down to $z=0$, with the aim of assessing how well the bright high redshift QSOs population traces the progenitors of most massive haloes in the local Universe. Our results show that at $z > 6$ bright QSOs live in a variety of environments, and that secular processes like disc instability are responsible for triggering roughly the same number of QSOs as galaxy mergers. Half of cubic ($7.5 h^{-1}$ cMpc size) mock fields built around these high- z QSOs include other active galaxies (with $L_{\text{bolo}} > 10^{44}$ erg/s) in sizeable number, the other host galaxies being relatively isolated. The large field-to-field variance in the number of companions (both active and non-active) recently reported from JWST observations is fairly well reproduced by GAEA predictions. Descendants of host galaxies at $z=0$ cover a wide range of physical properties and environments with only a small fraction of the hosts of high- z QSOs ending up in massive galaxy clusters. Viceversa, GAEA predicts that only a small fraction of Bright Central Galaxies have a bright $z > 6$ QSOs among their progenitors. Our results suggest that luminous high- z QSOs loosely trace the progenitors of low- z galaxy clusters, and that additional information about the environment of high- z QSOs are required to identify the most promising proto-cluster candidates.

Key words. galaxies: formation – galaxies: evolution – galaxies: active – galaxies: high redshift – galaxies: statistics

1. Introduction

Quasars (QSOs) observed in the first Gyr of the Universe ($z \gtrsim 5.7$) are among the most active sources emerging from the dark cosmic ages. They are characterized by rapid accretion rates ($\dot{M} > 10 M_{\odot} \text{ yr}^{-1}$) onto black holes that have already assembled masses as large as $10^9 M_{\odot}$, and by intense episodes for star formation (with rates $\text{SFR} = 100\text{--}1000 M_{\odot} \text{ yr}^{-1}$) fueled by copious reservoirs ($10^{10} M_{\odot}$) of molecular gas (see Fan et al. 2023 for a recent review).

In order to explain this rapid growth of both black holes and their host galaxies, a common broad-brush picture postulates that these sources reside at the core of some of the most prominent overdensities emerging at these early cosmic ages, often called “proto-clusters” (see Overzier 2016 for a review). Observational support to this hypothesis has been elusive, due to limitations on sensitivity, size of the field of view, sample sizes, and contradictory findings connected with selection effects (see discussions in Overzier et al. 2009 and Mazzucchelli et al. 2017). The first spectroscopic confirmations of galaxies in the close environment of QSOs at $z \gtrsim 5.7$ came from the Atacama Large Millimeter Array (Decarli et al. 2017; see also Trakhtenbrot et al. 2017; Willott et al. 2017, Neeleman et al. 2019) and from integral field spectroscopy with MUSE on the Very Large Telescope (Farina et al. 2017, Meyer et al. 2022).

While instrumental to demonstrate that (at least some) high- z QSOs do live in rich environments, these studies could only

probe the close, $\lesssim 100$ kpc, scales. This leaves an open question: are these companions a reflection of small-scale clustering (as expected in the case QSO activity is triggered by close galactic interactions), or are they the “peak of the iceberg”, i.e., the highest density regions of the large-scale structures hosting the QSOs? Only in the last few years, we have been able to address this question thanks to the superb slit-less spectroscopy capabilities of JWST. Kashino et al. (2023), Wang et al. (2024), Champagne et al. (2025) and Wang (2025) presented studies of the ~ 10 Mpc² area around QSOs at cosmic dawn. The NIRCam Wide Field Slit-less Spectroscopy (WFSS) mode delivered spectra of the rest-frame blue optical emission of all the sources in the targeted QSO fields. Via the bright [OIII] and H β line emission, the identification of the properties of galaxies around the QSOs is straightforward. These new campaigns have revealed tens of companion galaxies at separations as large as a few Mpc from the QSO. Significant field-to-field variation has been reported (Kashino et al. 2023). Eilers et al. (2024) used the statistics of companion galaxies around $z \gtrsim 5.7$ QSOs to estimate the QSO–galaxy correlation function and infer the mass of the host dark matter halo (DMH). They found a minimum host halo mass of $\log M_{\text{halo}}/M_{\odot} = 12.43^{+0.13}_{-0.15}$.

If QSOs reside in prominent structures in the first Gyr since the Big Bang, it is tempting to postulate that they mark the seeds for massive proto-clusters before cosmic noon and giant galaxy clusters in the local Universe (see e.g. Stiavelli et al. 2005; Dannerbauer et al. 2014; Morselli et al. 2014; Hennawi et al. 2015; Cucciati et al. 2018; Shah et al. 2024). Furthermore, the tumul-

* e-mail: fabio.fontanot@inaf.it

tuous growth of black holes and their hosts in the early Universes is expected to be connected with a rapid depletion of cold gas that would otherwise be used at later times. Hence, QSO hosts are often thought to represent the progenitors of massive and passive galaxies, and perhaps of bright central dominant galaxies. These speculative arguments can be quantitatively tested by means of theoretical models of galaxy evolution. However, such studies require large cosmological volumes to sample the range of possible environments and evolutionary paths of such rare objects. Semi-Analytic model (SAMs) represent an ideal framework for this analysis, as they provide a fast and computationally efficient approach to galaxy evolution, aimed at following the main physical properties of galaxy populations over a wide redshift range.

In this paper, we take advantage of the latest version of the GALaxy Evolution and Assembly (GAEA) model (De Lucia et al. 2024), featuring an advanced modelling for gas accretion onto Super-Massive Black Holes (SMBHs) at the centre of galaxies. In Fontanot et al. (2020), we showed that this approach is able to reproduce the space density evolution of the Active Galactic Nuclei (AGN) population at $z \lesssim 4$ in different luminosity ranges (the so-called AGN-downsizing). De Lucia et al. (2024) showed that our modelling of gas accretion and AGN feedback is instrumental (altogether with the improved modelling of star formation based on the partition of cold gas into its atomic and molecular components – Xie et al. 2017) to reproduce the observed fractions of quenched galaxies over a wide range of cosmic epochs. In Grazian et al. (2024), GAEA predictions have been compared with a detailed determination of the observed AGN luminosity function at $z \sim 5$, showing a good agreement with data. In a recent work, Cammelli et al. (2025) coupled a modified version of the GAEA model with predictions from fast methods based on the Lagrangian Perturbation Theory (Monaco et al. 2002) to study the properties of the high- z AGN population. While the aim of this work was to explore the impact of different BH seeding mechanisms on the galaxy/AGN populations, it has also provided some predictions for the expected space densities and for the shape of the relation between the mass of the SMBH (M_{BH}) and the stellar mass of the host galaxy (M_{\star}). The main limitation of the Cammelli et al. (2025) work with respect to the questions addressed here is the limited size of the simulated box. In this paper, we will use the PLANCK MILLENNIUM simulation (Baugh et al. 2019, PMS hereafter), that spans a volume of $\sim 0.5 \text{ Gpc}^3$. The PMS allows us to explore a cosmological volume large enough to detect a sizeable sample of bright QSOs at high- z , study the physical properties of their host galaxies and explore their evolution to lower redshift.

This paper is organized as follows. In Section 2 we present the GAEA model run on merger trees extracted from the PMS simulation, while in Section 3 we discuss the definition of a reference high- z mock sample. In Section 4 we present our results on the environment of high- z QSOs in GAEA and compare with recent observational determinations. Then in Section 5 we study the lower redshift evolution of high- z QSOs and in Section 6 we focus on the properties of their descendants. Finally, we summarize our conclusions in Section 7.

2. Galaxy formation model

In this study we consider predictions from the latest rendition of the GALaxy Evolution and Assembly (GAEA) model (see De Lucia et al. 2024, and references therein). Semi-analytic models (SAMs) are theoretical tools aimed at providing predictions for the growth of galaxy populations across cosmic epochs, start-

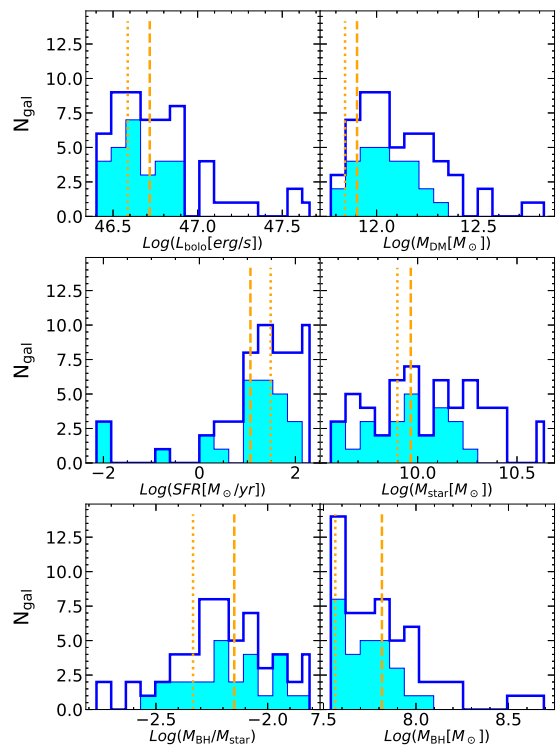


Fig. 1. Properties of the most luminous $z > 6$ QSOs and their host galaxies in GAEA. Blue empty histograms refer to the properties of the full sample of 56 high- z QSOs, while the cyan filled histograms show the same properties for the subsample of QSOs triggered by disc instability events. Vertical dashed and dotted lines mark the position of our reference objects (see main text for more details).

ing from a statistical description of the evolution of DMHs in a cosmological volume. Indeed, DMHs are assumed to be a natural cradle, where galaxies form from the baryonic gas accumulated into their potential wells and evolve under the effect of a complex network of physical mechanisms that drive the consumption of the cold gas reservoir either by forming stars or by accretion onto Super-Massive Black Holes (SMBHs) and the energy release via feedback effects. The approach relies on approximated parametrizations (empirical, numerical or purely theoretical in nature) to model the key physical processes. The lack of an explicit treatment of the gas dynamics largely reduces the numerical requirements, thus allowing for a detailed exploration of the parameter space associated with the assumed prescriptions. A SAM cannot track the spatial distribution of the different baryonic components (to the level of detail offered by a hydro-simulation), nonetheless, it is an ideal tool to explore galaxy evolution over a cosmological volume and across all cosmic epochs, providing the needed flexibility to study the impact of individual physical mechanisms.

De Lucia et al. (2024, see also Xie et al. 2024) introduced the latest version of the GAEA model, featuring a much needed synthesis of independent developments. In particular, this version of the model builds on the original model presented in Hirschmann et al. (2016) and includes (i) the explicit partition of cold gas into atomic and molecular component presented in Xie et al.

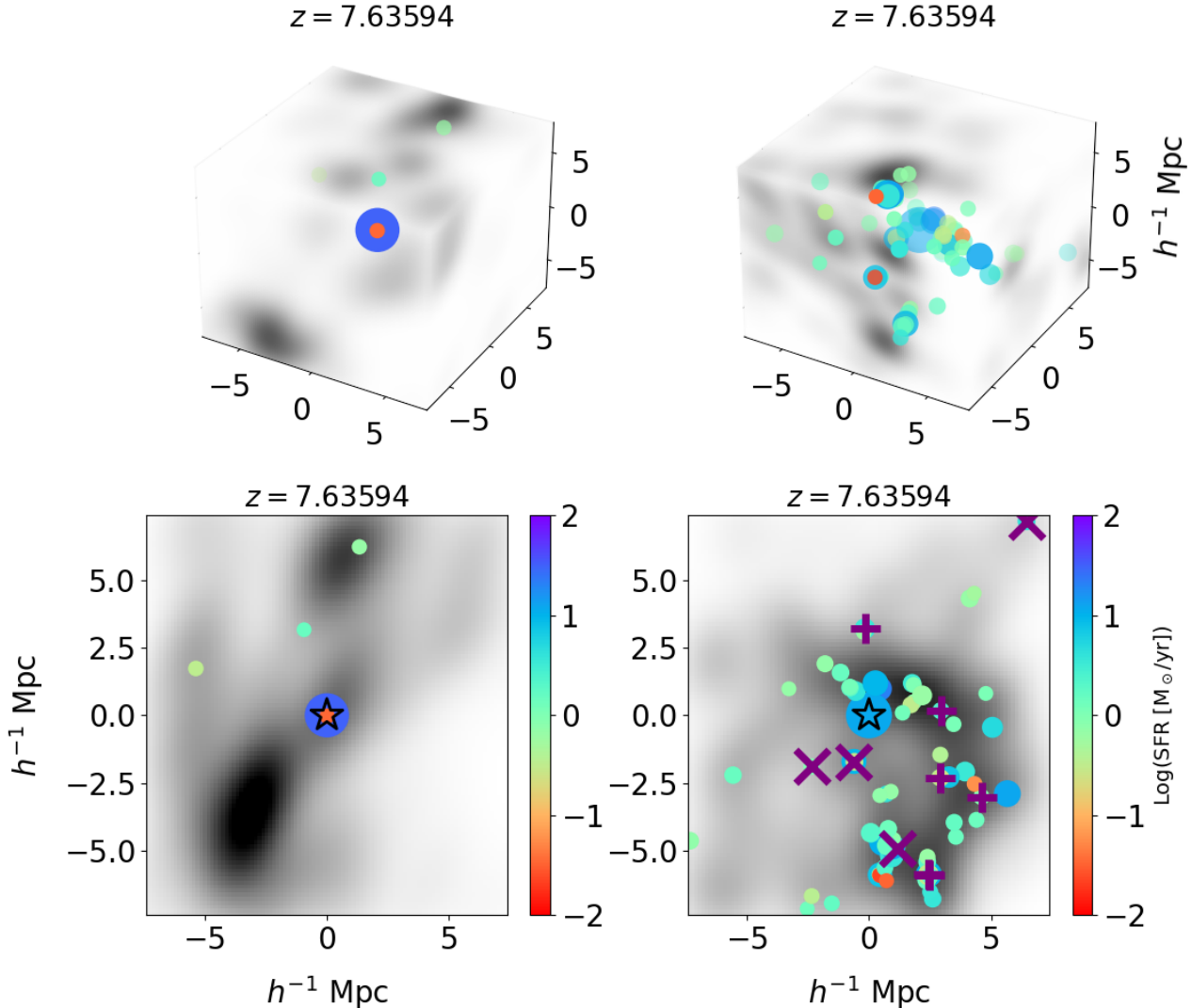


Fig. 2. *Upper panels:* 3D galaxy distribution around two representative high-z QSOs. Left-hand panels correspond to QSO-B, while right-hand panels to QSO-A (see text for more details). Circles mark the position of galaxy companions with $M_\star > 10^8 M_\odot$ in a $7.5 h^{-1}$ cMpc size box centred on the high-z QSO. The size of the symbols is proportional to the galaxy stellar mass, and they are colour coded according to their SFR as in the colorbar on the right of the lower panels. *Lower panels:* projected galaxy distribution around reference high-z QSOs. The depth of the projection is $7.5 h^{-1}$ cMpc. Purple pluses and crosses mark the position of AGN companions with $L_{\text{bol}} > 10^{42.5}$ erg/s and 10^{44} erg/s, respectively. In all panels, the grey shading correspond to the underlying projected distribution of dark matter, computed from the distribution of DMHs in the simulated volume.

(2017), (ii) the modelling of cold gas accretion onto SMBHs and AGN feedback from Fontanot et al. (2020) and (iii) the treatment of dynamical processes acting on satellite galaxies described in Xie et al. (2020). This new version of the model has been calibrated against the evolution of the galaxy stellar mass function up to $z \sim 3$; the evolution of the AGN luminosity function up to $z \sim 4$ and the local HI and H_2 mass functions. Our previous work has shown that this realization correctly tracks the fractions and space densities of quiescent galaxies up to $z \sim 4$ (De Lucia et al. 2024), the emission line properties of different galaxy populations (Euclid Collaboration et al. 2024), the clustering properties of galaxy populations as a function of stellar mass, star formation activity, HI content and redshift (Fontanot et al. 2025). In a recent paper, Cantarella (2025) tested GAEA predictions against the

latest JWST measurements of the Ultra-Violet luminosity functions at $z > 5$ and of the evolution of the mass-metallicity relation finding reasonable agreement for model predictions with both observational determinations up to $z \sim 9-10$.

In the following we will consider the most recent GAEA realization (Fontanot et al. 2025), that takes advantage of the coupling of the model with merger trees extracted from the PMS. The PMS tracks the evolution of the Large Scale Structure in a 800^3 Mpc 3 volume assuming a cosmological model ($\Omega_\Lambda = 0.693$, $\Omega_m = 0.307$, $\Omega_b = 0.04825$, $n = 0.9611$, $\sigma_8 = 0.8288$, $H_0 = 67.77$ km/s/Mpc) based on the first year results from the Planck satellite (Planck Collaboration XVI 2014). This numerical simulation has been run using a reduced memory version of the N-body code GADGET (Springel et al. 2005)

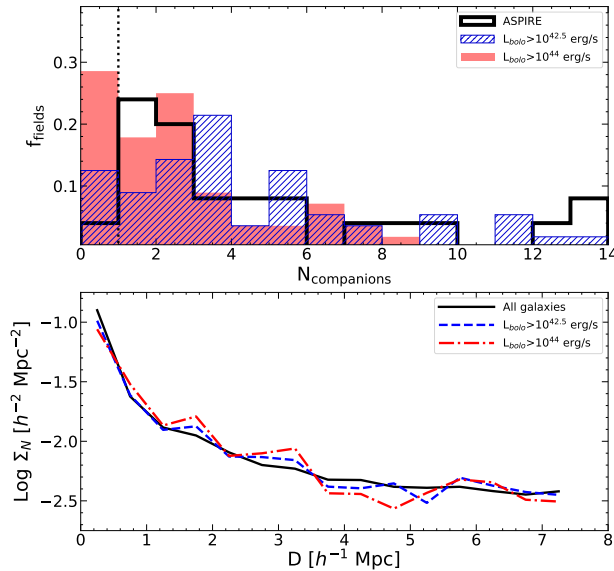


Fig. 3. *Upper panel:* Fraction of fields f_{fields} hosting a given number of $M_{\star} > 10^8 M_{\odot}$ AGN companions brighter than $L_{\text{bolo}} > 10^{42.5}$ (blue dot-dashed histogram) and 10^{44} erg/s (red dashed histogram and Orange filled area). The black histogram shows the fraction of fields in the ASPIRE survey, hosting a given number of $[\text{O}_{\text{III}}]$ emitters (Wang 2025). *Lower panel:* $M_{\star} > 10^8 M_{\odot}$ galaxy surface number density distribution as a function of projected galaxy separation from the central QSO. Solid black, red dashed and blue dot-dashed lines refer to the total galaxy population and the AGN companions (defined using a with $L_{\text{bolo}} > 10^{42.5}$ and 10^{44} erg/s AGN luminosity threshold) respectively.

and approximately 128 billion particles to recover the assembly of the DMHs, resulting in a particle mass resolution of $1.06 \times 10^8 h^{-1} M_{\odot}$; running GAEA on the PMS merger trees thus allow us to resolve the physical properties of model galaxies more massive than $10^8 M_{\odot}$. Predictions of the GAEA realization on the PMS have been shown to be consistent with results from runs over other cosmological simulations belonging to the same suite, such as the MILLENNIUM and MILLENNIUM-II (with different mass resolution and assuming slightly different cosmological parameters), at fixed SAM parameters (see Fontanot et al. 2025, for details). This improved convergence of model predictions with respect to previous versions of the code is due to the interplay between physical mechanisms acting as regulators of the cold gas content of model galaxies, namely the cold gas accretion onto the central SMBH (as described in Fontanot et al. 2020), the star formation based on the partition of cold gas (Xie et al. 2024) and the corresponding AGN and stellar feedbacks.

Given the focus of this work, we will briefly recap the main features of the modelling of gas accretion onto SMBHs in GAEA. We refer the interested reader to Fontanot et al. (2020) for a detailed description of the model and its main predictions. First of all, we assume a flat BH seeding scheme: each time a new DMH is resolved (at $2 \times 10^9 h^{-1} M_{\odot}$, corresponding to 20 simulated DM particles) in the merger tree, we seed it with a $\sim 10^2 M_{\odot}$ BH. We assume that AGN activity is triggered by physical processes able to destabilize the cold gas in star forming galaxy discs, make it lose its angular momentum and infall towards the centre of the galaxy to form a reservoir around the SMBH. In GAEA we assume that either galaxy mergers or secular processes like disc

instabilities are possible triggers. Whenever one of these processes occurs, we take a fraction of the cold gas available in the model galaxy and we move it into a reservoir around the central SMBH. The fraction of cold gas involved is modulated by the expected SFR. The gas accretion from the reservoir onto the SMBH is regulated by a viscous accretion timescale (Umemura 2001; Granato et al. 2004) and limited to a maximum value of 10 times the Eddington rate. Finally, AGN activity is assumed to provide feedback to the host galaxy, by means of AGN-driven outflows, characterized by a mass loading factor proportional to the SMBH accretion rate. Bolometric luminosities for our model AGNs have been computed from the corresponding accretion rates assuming a 15 per cent radiative efficiency.

3. Selection of high-z QSOs in GAEA

We extract a sample of high-z QSOs using the following selection. We first select all QSOs at $z > 6$ with bolometric luminosity above a threshold of $L_{\text{bolo}} > 10^{46.25}$ erg/s. We then select among those all model galaxies with Black Hole mass $M_{\text{BH}} > 10^{7.5} M_{\odot}$ and stellar mass $M_{\star} > 10^9 M_{\odot}$, ending up with a sample of 56 systems at $6 < z < 8$. These cuts are meant to select the most extreme objects hosting an accreting SMBH at high redshift. It is worth stressing that this sample does not include all $M_{\star} > 10^9 M_{\odot}$ galaxies in this redshift range. Among these 56 sources, only 2 are satellite galaxies (their corresponding central galaxies are not in the sample). For each high-z QSO we consider their local environment, by selecting all galaxies closer than $7.5 h^{-1} \text{ Mpc}$ (comoving), at the redshift of detection. Finally, for each of our selected high-z QSOs we reconstruct the redshift evolution of the main progenitor and descendant along the corresponding merger trees, in order to infer the various evolutionary paths and identify the low-z counterparts.

In Fig. 1, the blue histograms show the distribution of the main properties of the QSO host galaxies at the redshift of detection. These histograms show that high-z QSO hosts cover a relatively wide interval both in M_{\star} and in M_{DM} . Moreover, the selection follows closely the BH mass function, while the histograms as a function of L_{bolo} and M_{\star} are shallower than the corresponding bolometric luminosity function or the galaxy stellar mass function. Most of the objects are relatively star-forming and tend to lie above the local $M_{\text{BH}} - M_{\star}$ relation. A critical point in the GAEA framework involves the triggering mechanisms for the AGNs, i.e. the relative role of disc instabilities and mergers in sustaining the accretion onto the SMBHs. It is worth noting that at such high redshift it is not always possible to split GAEA model galaxies in a clear way between the two triggering channels. In fact, we found in a significant fraction of the sources a contribution of both channels to the same event. For example, the dominant effect of a minor merger to the accretion event might not be the direct channelling of cold gas to the centre. Indeed, in GAEA the cold gas content of the satellite is given to the cold gas disc of the remnant, which could then trigger a series of disc instability events that bring additional cold gas to the reservoir around the central SMBH. We include all events that start with a merger under the ‘‘merger’’ label, even if most of the cold gas content may be brought by the subsequent disc instabilities. According to these definitions roughly half of the our high-z QSO sample is triggered by disc instability events. The cyan filled histogram refer to the distribution of the properties of host galaxies for the subsample of QSO triggered by disc instability only events. Overall, the comparison of the blue and cyan histograms suggests that the most luminous events involving the more massive SMBHs are mostly connected to galaxy mergers.

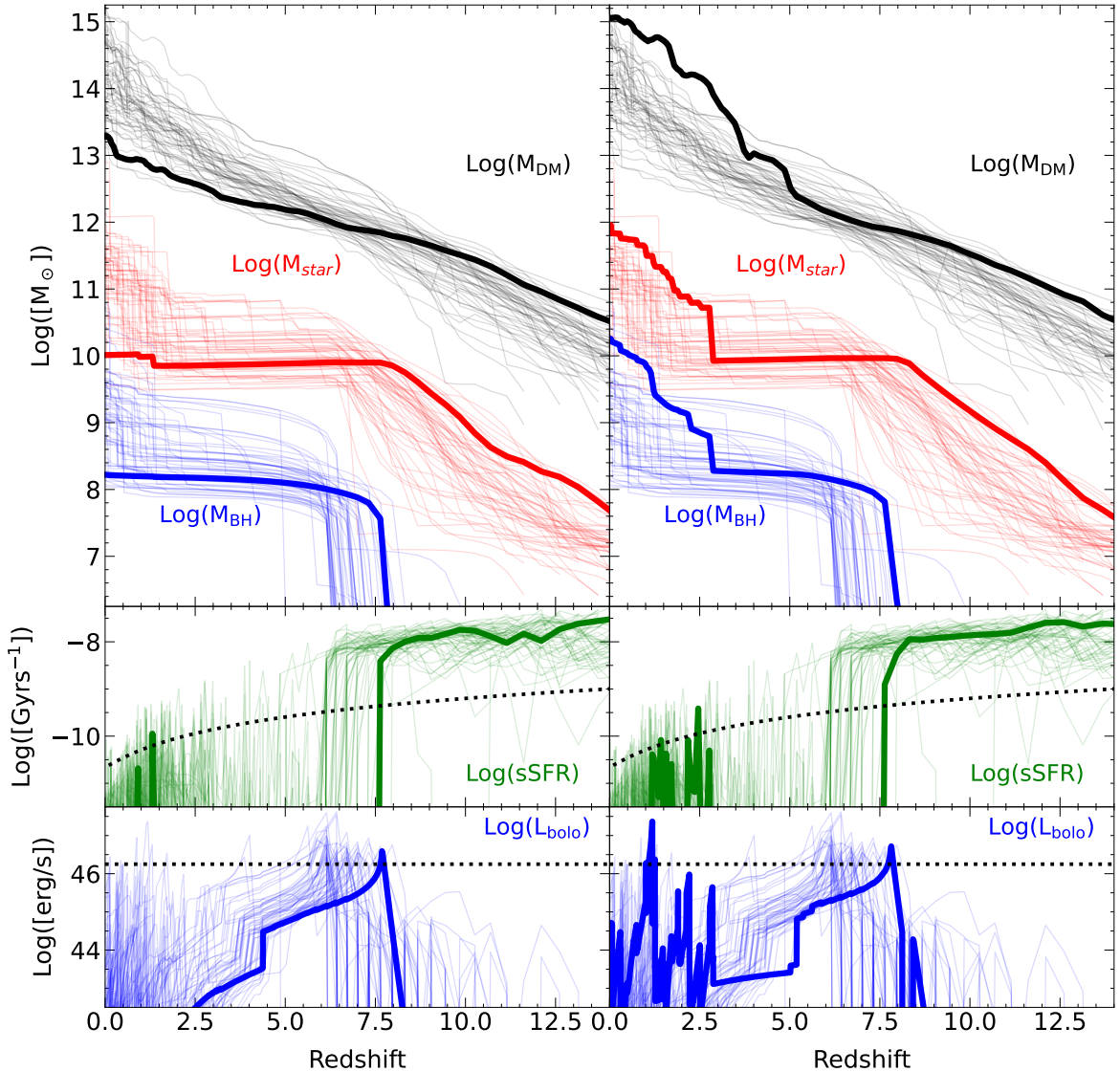


Fig. 4. Redshift evolution of selected properties of the host galaxies for the two reference high-z QSOs (thick lines). In all panels, the evolutionary tracks for the entire sample of high-z QSOs is shown with thin lines. Left Panels correspond to the redshift evolution for QSO-B, while the right panel for QSO-A (see text for more details). Upper panels show the redshift evolution of the parent DMH mass, stellar mass and SMBH mass. Lower panels show the redshift evolution for the sSFR and bolometric luminosity. In the sSFR panel, the dotted line represent a classical threshold for defining active galaxies in theoretical models, larger than $0.3/t_H$, where t_H is the Hubble time at the redshift under consideration. In the L_{bolo} panel, the horizontal line marks the detection threshold for high-z QSOs we assume in this work.

4. Environment of high-z QSOs in GAEA

We then consider the environment of high-z QSOs. We isolated two broad categories to classify high-z QSOs (although a continuous distribution of cases is in place): the first one includes galaxies that already reside at the centre of a galaxy overdensity. This implies a large number of companion galaxies and a relevant chance for later galaxy growth via mergers and interactions. A second possibility involves a host galaxy living in a relative isolation already at high-z (a small number of compan-

ion galaxies). We stress that this separation is only qualitative, and all possible intermediate configurations are found in our selected sample. As an illustration, we select two representative galaxies of these groups and we show in Fig. 2 the distribution of companion galaxies with $M_\star > 10^8 M_\odot$, in a box with size $7.5 h^{-1}$ cMpc centred on the high-z QSO. These two sources have been selected at the same redshift ($z \sim 7.5$) and roughly at the same $L_{\text{bolo}} \sim 10^{46.6}$ erg/s. In the upper panels we show the tridimensional distribution around the selected high-z QSO, while in

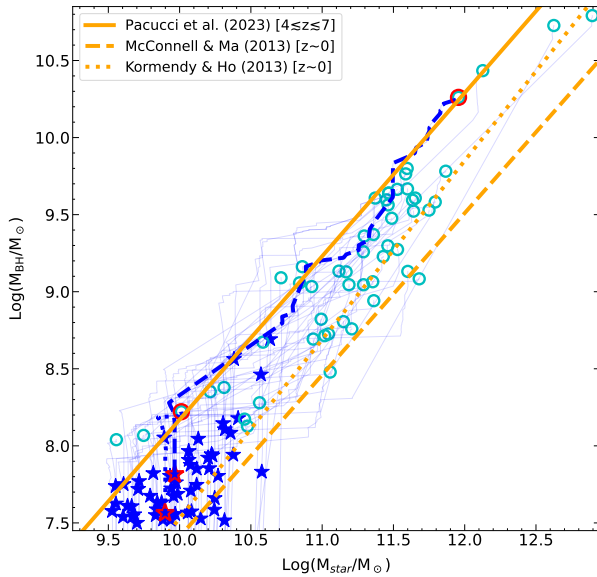


Fig. 5. Evolution of the $M_{\text{BH}}-M_{\star}$ relation for the host galaxies of high-z QSOs. Blue stars represent the relation at the redshift of detection of the sample, while cyan circles mark the position at $z \sim 0$. Thin lines show the evolution of the relation along the main progenitor of the host galaxy. Red open symbols and blue thick lines show the evolution for QSO-A and QSO-B (dotted and dashed line respectively). Orange lines refer to observed relations at different redshifts, as estimated by [Pacucci et al. \(2023, at \$4 < z < 7\$ \)](#), [Kormendy & Ho \(2013, at \$z \sim 0\$ \)](#) and [McConnell & Ma \(2013, at \$z \sim 0\$ \)](#).

the lower panels we show an arbitrary 2d projection (the depth of the projection still correspond to $7.5 h^{-1} \text{ cMpc}$). In each panel the size of the points is proportional to the stellar mass of the model galaxy, and each of them is colour-coded according to its SFR, as indicated in the the colorbar on the right of each panel. The QSO host on the right (QSO-A hereafter) lives in what is already a galaxy overdensity that will evolve into a massive cluster at $z \sim 0$ (see following analysis), while the galaxy on the left (QSO-B hereafter) lives in isolation and its activity has been triggered by a disc instability event in a gas rich galaxy disc. In the lower panels, we show the corresponding projected distribution of sources on x-y plane. In these plots we also mark the position of active companions with crosses and pluses (defined as those sources with L_{bolo} larger than $10^{42.5} \text{ erg/s}$ and 10^{44} erg/s , respectively). In each panel of Fig. 1, the physical properties of QSO-A and QSO-B are marked by vertical dashed and dotted lines respectively: they lie relatively close to each other for a number of properties (the hosted M_{BH} showing the largest separation).

For a more quantitative analysis on the distribution of these active companions, we show in Fig. 3 (upper panel) the classification of the 56 mock fields as a function of number of $M_{\star} > 10^8 M_{\odot}$ companions N_{comp} , for the same two cuts in L_{bolo} we previously considered. In particular, we show in the upper panel, the fraction of the mock fields hosting a given number of AGN companions. There are typically less than 3 companions brighter than 10^{44} erg/s , while when considering a lower luminosity cut ($10^{42.5} \text{ erg/s}$), the number of companions can vary significantly ranging from zero to more than 10. GAEA predicts that almost half of the fields centred around high-z QSOs should contain at least 2 bright ($L_{\text{bolo}} > 10^{44} \text{ erg/s}$) QSOs. This figure is

increased to ~ 80 percent of the fields for the fainter threshold. It is worth stressing that, at least for the fainter AGN sample, the actual numbers depend on the stellar mass limit assumed for the mock sample, which in our case corresponds to $M_{\star} > 10^8 M_{\odot}$. We contrast model predictions with the results from the ASPIRE program ([Wang 2025](#)), a galaxy redshift survey targeting fields around $25 z \gtrsim 6.5$ QSOs with JWST and ALMA. ASPIRE has been able to detect O_{III} emitters both along the line of sight and close to the reference source. One of the key findings of the program is the fact that the number of companion O_{III} emitters varies significantly from field to field, suggesting a quite different QSO environment, in good agreement with our findings. It is worth stressing that the O_{III} line survey selects a mixed population including both star-forming galaxies and AGNs: additional emission lines would be necessary to disentangle sources dominated by emission from the central BH. In general, one may expect the brightest emitters to be AGN dominated, but at the assumed selection threshold for the survey (i.e. $L_{\text{bolo}} > 10^{42} \text{ erg/s}$), an important contribution of star-forming galaxies has to be taken into account. Nonetheless, ASPIRE results can be considered a benchmark for the study of the number of galaxy companions around high-z QSOs: in the upper panel of Fig. 3 we report the fraction of ASPIRE fields hosting a given number of O_{III} emitters as black histogram. The comparison with the predicted distributions for GAEAAGN companions shows a general qualitative agreement, which is still rather intriguing, despite the different selections between data and mocks. Moreover, it is important to keep in mind that not only the selection of the samples is different (i.e. AGNs versus O_{III} emitters), but also the definition of surveyed volumes are quite different between the survey and the mock catalogues, and the GAEA selection relies heavily on stellar mass, while in ASPIRE it is based only the O_{III} lines luminosity.

We also consider the mean projected number density of $M_{\star} > 10^8 M_{\odot}$ companions galaxies in our mock fields (Fig. 3 - lower panel). Black solid, blue dashed and red dot-dashed lines show the resulting distributions as a function of distance from the reference QSO for the all companions (both active and inactive) and for AGN companions above the usual luminosity thresholds. All distributions have been rescaled to the total number of sources to ease the comparison. The results highlight that AGN companions do not show any clear signal for a different distribution (i.e. a stronger clustering) with respect to the overall galaxy population around these high-z QSOs.

5. Redshift evolution

We then consider the evolutionary history of the high-z QSO host galaxies as predicted by GAEA. In Fig. 4, we collect all evolutionary tracks for the 56 objects in our sample (light lines). In detail, we consider the redshift evolution of mass components (M_{DM} , M_{\star} , M_{BH}), as well as the evolution of the specific SFR ($\text{sSFR} = \text{SFR}/M_{\star}$) and L_{bolo} . Overall, these evolutionary tracks span a wide range of possible histories, both in terms of mass assembly and activity. In Fig. 4 we also highlight with bold lines the tracks corresponding to the same two representative sources selected in Fig. 2. We stress again that these two objects have quite similar properties at the detection redshift ($z \sim 7.5$), for most of the quantities shown in Fig. 4: however their evolution at lower redshift is strikingly different. In the left-hand panels, we show that the evolution for QSO-B after the main triggering event (a disc instability) is rather quiet, the host galaxy rapidly becomes quiescent and it does not form stars at a relevant rate at later times. Despite being one of the most massive systems in the box at $z \sim 7.5$

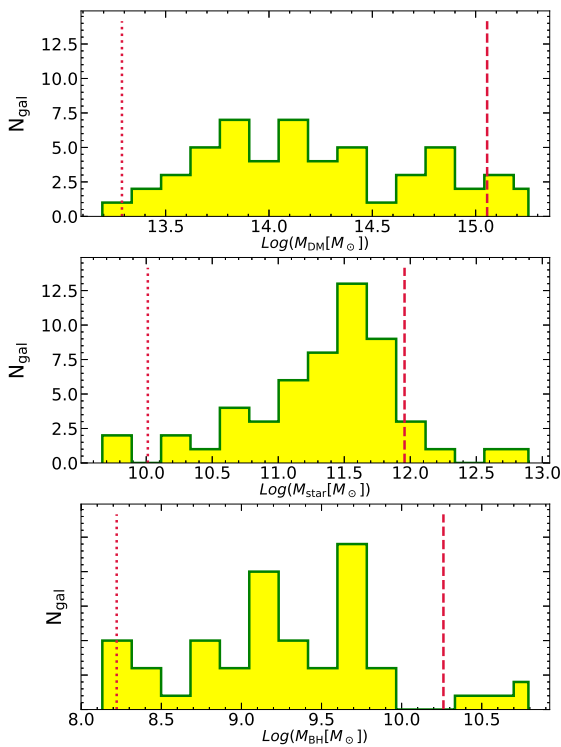


Fig. 6. Properties for main descendants of high-z QSO hosts. Vertical dashed and dotted lines mark the properties of QSO-A and QSO-B descendants.

with $M_\star \sim 10^{10} M_\odot$, the host galaxy does not grow significantly in mass down to $z=0$.

In the right-hand panels of Fig. 4 we show QSO-A, living in a more dense environment at $z\sim 7.5$, and characterized by a more complex evolutionary history. Also for this source the main triggering event is a disc instability¹. The host galaxy is rapidly quenched (similarly to QSO-B) and does not form stars at a relevant rate down to $z\sim 2.5$ (thus being detectable as a massive red and dead galaxy in this redshift interval). Then it suffers a series of merger events, leading to the formation of a Bright Central Galaxy (BCG) of a $M_{\text{DM}} \sim 10^{15} M_\odot$ galaxy cluster. This merger series is also associated to a very bright QSO phase at $z\sim 1$. It is worth noting that during this merger phase the high-z QSO host galaxy does not correspond to the most massive galaxy in its environment (i.e. the main progenitor of the BCG). We stress that the two examples shown in Fig. 4 are representative for extreme scenarios. Indeed, the ensemble of light lines in Fig. 4, highlights the intrinsic stochasticity of mass assembly in a hierarchical Universe (see e.g. De Lucia & Blaizot 2007; Trenti & Stiavelli 2008; Overzier et al. 2009; Angulo et al. 2012).

We also consider the position of our model galaxies in the $M_{\text{BH}}-M_\star$ plane in Fig. 5. Most of our bright high-z QSOs (blue stars) lie above the local relation (McConnell & Ma 2013 and/or Kormendy & Ho 2013), while a handful of them are in agree-

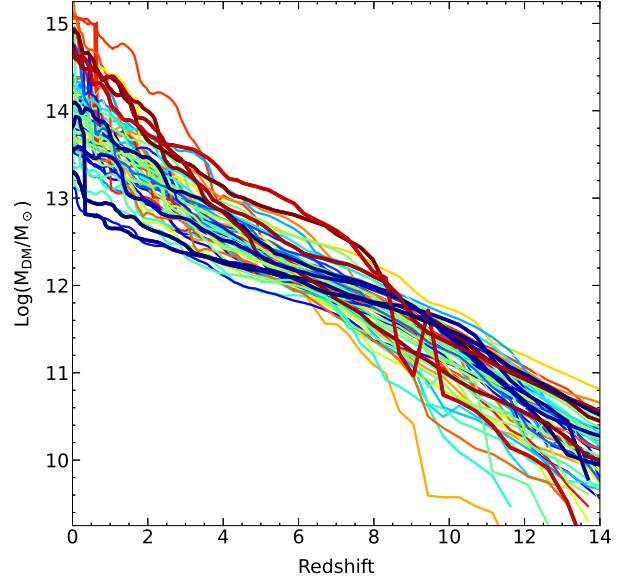


Fig. 7. Redshift evolution of parent halo mass (M_{DM}) of the host galaxies for our sample of high-z QSOs. Individual tracks are progressively coloured from dark blue to dark red at increasing number of total companions with $M_\star > 10^8 M_\odot$ at the detection redshift. Thicker blue and red lines correspond to the 4 model AGNs with less and more companions, respectively.

ment with the Pacucci et al. (2023) relation. At high redshift, all selected model QSOs show a faster growth in M_{BH} than in M_\star , which brings them above the local relation. Objects like QSO-A do not evolve any further at lower redshifts, while sources like QSO-B tend either to evolve parallel to the local relation (if they have lower-z reactivation events), or move back to the local relation (if their evolution is dominated by galaxy mergers with no additional bright QSO events). At $z\sim 0$ the descendants of the high-z QSOs (cyan circles) represent a galaxy population whose SMBH tend to lie above the local $M_{\text{BH}}-M_\star$ relation, although a significant fraction of ~ 60 per cent is within the quoted 0.3 dex around the observed relation.

6. The relation between high-z QSO and local Large Scale Structure

In order to better quantify the relationship between high-z QSOs and their evolution into the galaxy population at $z\sim 0$, we show the distribution of some selected properties of their descendant galaxies at $z\sim 0$ in Fig. 6. When considering the properties of the descendant population, the final distributions for the mass components (M_{DM} , M_\star , M_{BH}) are still quite broad. As already discussed in our previous analysis, QSO-A and QSO-B lie at the extremes of the $z\sim 0$ distributions. Our main conclusions do not change if we restrict the sample of model galaxies only to the hyper-luminous QSOs (i.e. $L_{\text{bolo}} > 10^{47} \text{ erg/s}$, see also Salvestrini et al. 2025). Only 32 out of 56 objects in our sample (57 per cent) end up in galaxy clusters ($M_{\text{DM}} > 10^{14} M_\odot$) at low redshift, while the remaining fraction lives in massive groups ($M_{\text{DM}} > 10^{13} M_\odot$). Moreover, our sample does not trace all the more massive structures in the simulation box. Indeed, we identify 45 galaxy clusters with $M_{\text{DM}} > 10^{15} M_\odot$ in the PMS at $z=0$. Only 4 of these include descendants of high-z QSOs (such as QSO-A), which cor-

¹ We stress that our results are independent of the triggering mechanism, i.e. it would be possible to select two analogous merger-triggered high-z QSOs from our sample.

responds to only 9 per cent of the $z=0$ galaxy clusters². None of the high- z QSO in our sample is the main progenitor of a central BCG, but rather belongs to another structure merging with the main progenitor of the cluster halo at later times. Therefore, even if not the more massive galaxy along the evolutionary path of the BCG, the high- z QSO usually belongs to the more active evolutionary branch. However, it is quite telling, that the largest fraction (more than 90 percent) of $z\sim 0$ $M_{\text{DM}} > 10^{15} M_{\odot}$ clusters in the PMS, do not include any galaxy corresponding to the descendant of our bright high- z QSOs. We study the evolution of the properties of the BCG at different epochs and we find that the main reason for this is that their more active phase typically peaks at lower redshift (in a large $z\sim 3\text{-}5$ range) than our selection at $z>6$. Moreover, 8 high- z QSO in our sample (14 per cent) correspond to a satellite descendant at $z=0$, and 2 of them (3.5 per cent) to an orphan galaxy (i.e. a model satellite galaxy whose substructure has been stripped below the resolution of the merger tree).

In order to understand how well the properties of high- z QSOs in `GAEA` can predict the $z\sim 0$ environment of their descendants, we consider in Fig. 7 the same M_{DM} evolutionary tracks considered in Fig. 4, and we colour code them from dark blue to dark red with increasing number of $M_{\star} > 10^8 M_{\odot}$ companions at detection redshift. Fig. 7 suggests that high- z environments defined by a larger (smaller) number of companion galaxies show a tendency to end in more massive (less massive) haloes at lower redshift. Similar results hold if we use the number of active companions (at both L_{bolo} thresholds we considered). We stress that these results represent a general prediction for the hierarchical assembly of the Large Scale Structure (see e.g. Angulo et al. 2012); in a forthcoming paper (De Lucia 2025), we will expand this analysis to the environment of massive ($M_{\star} \gtrsim 10^{11} M_{\odot}$) $3 < z < 5$ galaxies.

7. Summary

In this paper, we present predictions from the latest version of the `GAEA` model, run on merger trees extracted from the `PLANCK MILLENIUM` simulation. We focus our analysis on a sample of mock $z>6$ QSOs, defined as sources with $L_{\text{bolo}} > 10^{46.25} \text{ erg/s}$; $M_{\text{BH}} > 10^{7.5} M_{\odot}$ and $M_{\star} > 10^9 M_{\odot}$. These selection cuts are meant to identify the most extreme objects in terms of SMBH accretion in our simulated box. We consider both the environment (defined as the number of companion galaxies within a cubic box of $7.5 h^{-1} \text{ Mpc}$ size) around the selected sources, as well as their lower redshift evolution. Our main results can be summarized as follows:

- * Bright high- z QSOs in `GAEA` are triggered in a variety of environments, ranging from galaxy overdensities that may collapse in galaxy clusters at $z\sim 0$, to galaxies evolving in relative isolation. Roughly half of the sources in our sample have been triggered by disc instability events. The brightest events in more massive galaxies and DM haloes originate from galaxy mergers.
- * Roughly half of the mock fields contain AGN companions with bolometric luminosity in excess of 10^{44} erg/s and stellar mass above our nominal resolution ($10^8 M_{\odot}$). These figures increase if a fainter luminosity threshold is adopted to select AGN companions (e.g. 80 percent for $L_{\text{bolo}} > 10^{42.5} \text{ erg/s}$).

² This figure decreases with M_{DM} , i.e. only 0.6 per cent of galaxy clusters with $M_{\text{DM}} > 10^{14} M_{\odot}$ and 2 per cent of galaxy clusters with $M_{\text{DM}} > 10^{14.5} M_{\odot}$ in the PMS include a descendant of a high- z QSO from our sample.

- * The evolution of the host galaxies of bright high- z QSOs show a high degree of variability and descendants are predicted to span a wide range of physical properties. All host galaxies have been quenched as the result of the QSO activity. Some of the selected sources do not experience other major star forming events after the main triggering event, thus ending up in a “red and dead” galaxy at lower redshifts. However, ~40 per cent of model sources are characterized by a rejuvenation phase, with subsequent star formation and AGN events at later times.
- * Local descendants of high- z QSOs live in a wide range of environments. Although they all live in $M_{\text{DM}} > 10^{13} M_{\odot}$, only a small fraction (4 out of 56, 7 percent) ends up in $M_{\text{DM}} > 10^{15} M_{\odot}$ clusters of the box. Conversely, only a small fraction (4 out of 45, 9 percent) of $z\sim 0$ $M_{\text{DM}} > 10^{15} M_{\odot}$ clusters in the PMS, have a bright high- z QSO within their progenitors. Our results suggests that observed bright high- z QSOs are poor tracers of the progenitors of local massive clusters, and additional information (such as the number and properties of their companions) is needed to select the most promising candidates.

These results are in qualitative agreement with recent finding from the `ASPIRE` program, which highlight a relevant field to field variation in the number of AGN companions around $z \gtrsim 6.5$ bright QSOs. Only for a fraction of the observed field, a large number of companions indicates the presence of an over-density. `GAEA` predictions do not support the assumption that the brightest ($L_{\text{bolo}} > 10^{46.25} \text{ erg/s}$) QSO found at $z>6$ are the signposts of the progenitors for the most massive $M_{\text{DM}} > 10^{14.5} M_{\odot}$ clusters at $z\sim 0$ (see also Overzier et al. 2009 and Eilers et al. 2024). The evolution of their hosts shows a variety of paths, which can be broadly tied to their high- z environment, defined as the number of (both active and inactive) companions in our mock fields. Despite a tendency for high- z QSOs with a large number of companions to end-up in massive structures at $z\sim 0$, we find that their host galaxies do not always correspond to the main progenitor of the more massive $z\sim 0$ galaxies in these large haloes in the PMS.

Acknowledgements. We thank Feige Wang for sharing results from the `ASPIRE` program. An introduction to `GAEA`, a list of our recent work, as well as datafile containing published model predictions, can be found at <https://sites.google.com/inaf.it/gaea/home>. We acknowledge the use of INAF-OATs computational resources within the framework of the CHIPP project (Tafoni et al. 2020) and the INAF PLEIADI program (<http://www.pleiadi.inaf.it>). FF, RD, GDL and OC acknowledge the support and hospitality of the Institute for Fundamental Physics of the Universe (IFPU), that has been instrumental for to the development of this work, under the Team Research Program “The environment of Quasars at the Cosmic Dawn” held on 17-21 February 2025. FF acknowledges support from the Next Generation European Union PRIN 2022 “20225E4SY5 - From ProtoClusters to Clusters in one Gyr”. RD acknowledges support from the INAF GO 2022 grant “The birth of the giants: JWST sheds light on the build-up of quasars at cosmic dawn”, and by the PRIN MUR “2022935STW”, RFF M4.C2.1.1, CUP J53D23001570006 and C53D23000950006.

References

Angulo, R. E., Springel, V., White, S. D. M., et al. 2012, MNRAS, 426, 2046
 Baugh, C. M., Gonzalez-Perez, V., Lagos, C. D. P., et al. 2019, MNRAS, 483, 4922
 Cammelli, V., Monaco, P., Tan, J. C., et al. 2025, MNRAS, 536, 851
 Cantarella, S. e. a. 2025, in preparation
 Champagne, J. B., Wang, F., Zhang, H., et al. 2025, ApJ, 981, 113
 Cucciati, O., Lemaux, B. C., Zamorani, G., et al. 2018, A&A, 619, A49
 Dannerbauer, H., Kurk, J. D., De Breuck, C., et al. 2014, A&A, 570, A55
 De Lucia, G. & Blaizot, J. 2007, MNRAS, 375, 2
 De Lucia, G., Fontanot, F., Xie, L., & Hirschmann, M. 2024, A&A, 687, A68
 De Lucia, G. e. a. 2025, in preparation

Decarli, R., Walter, F., Venemans, B. P., et al. 2017, *Nature*, 545, 457

Eilers, A.-C., Mackenzie, R., Pizzati, E., et al. 2024, *ApJ*, 974, 275

Euclid Collaboration, Scharré, L., Hirschmann, M., et al. 2024, *A&A*, 689, A276

Fan, X., Bañados, E., & Simcoe, R. A. 2023, *ARA&A*, 61, 373

Farina, E. P., Venemans, B. P., Decarli, R., et al. 2017, *ApJ*, 848, 78

Fontanot, F., De Lucia, G., Hirschmann, M., et al. 2020, *MNRAS*, 496, 3943

Fontanot, F., De Lucia, G., Xie, L., et al. 2025, *A&A*, 699, A108

Granato, G. L., De Zotti, G., Silva, L., Bressan, A., & Danese, L. 2004, *ApJ*, 600, 580

Grazian, A., Giallongo, E., Boutsia, K., et al. 2024, *ApJ*, 974, 84

Hennawi, J. F., Prochaska, J. X., Cantalupo, S., & Arrigoni-Battaia, F. 2015, *Science*, 348, 779

Hirschmann, M., De Lucia, G., & Fontanot, F. 2016, *MNRAS*, 461, 1760

Kashino, D., Lilly, S. J., Matthee, J., et al. 2023, *ApJ*, 950, 66

Kormendy, J. & Ho, L. C. 2013, *ARA&A*, 51, 511

Mazzucchelli, C., Bañados, E., Decarli, R., et al. 2017, *ApJ*, 834, 83

McConnell, N. J. & Ma, C.-P. 2013, *ApJ*, 764, 184

Meyer, R. A., Decarli, R., Walter, F., et al. 2022, *ApJ*, 927, 141

Monaco, P., Theuns, T., Taffoni, G., et al. 2002, *ApJ*, 564, 8

Morselli, L., Mignoli, M., Gilli, R., et al. 2014, *A&A*, 568, A1

Neeleman, M., Bañados, E., Walter, F., et al. 2019, *ApJ*, 882, 10

Overzier, R. A. 2016, *A&A Rev.*, 24, 14

Overzier, R. A., Guo, Q., Kauffmann, G., et al. 2009, *MNRAS*, 394, 577

Pacucci, F., Nguyen, B., Carniani, S., Maiolino, R., & Fan, X. 2023, *ApJ*, 957, L3

Planck Collaboration XVI. 2014, *A&A*, 571, A16

Salvestrini, F., Feruglio, C., Tripodi, R., et al. 2025, *A&A*, 695, A23

Shah, E. A., Lemaux, B., Forrest, B., et al. 2024, *MNRAS*, 529, 873

Springel, V., White, S. D. M., Jenkins, A., et al. 2005, *Nature*, 435, 629

Stiavelli, M., Djorgovski, S. G., Pavlovsky, C., et al. 2005, *ApJ*, 622, L1

Taffoni, G., Becciani, U., Garilli, B., et al. 2020, *arXiv e-prints*, arXiv:2002.01283

Trakhtenbrot, B., Lira, P., Netzer, H., et al. 2017, *Frontiers in Astronomy and Space Sciences*, 4, 49

Trenti, M. & Stiavelli, M. 2008, *ApJ*, 676, 767

Umemura, M. 2001, *ApJ*, 560, L29

Wang, F., Yang, J., Hennawi, J. F., et al. 2024, *ApJ*, 962, L11

Wang, F. e. a. 2025, in preparation

Willott, C. J., Bergeron, J., & Omont, A. 2017, *ApJ*, 850, 108

Xie, L., De Lucia, G., Fontanot, F., et al. 2024, *ApJ*, 966, L2

Xie, L., De Lucia, G., Hirschmann, M., & Fontanot, F. 2020, *MNRAS*, 498, 4327

Xie, L., De Lucia, G., Hirschmann, M., Fontanot, F., & Zoldan, A. 2017, *MNRAS*, 469, 968